THE JOURNAL OF BIOLOGICAL CHEMISTRY VOL. 286, NO. 43, pp. 37503–37514, October 28, 2011

Functional Extension of Amino Acid Triads from the Fourth Transmembrane Segment (S4) into Its External Linker in Shaker K^+ Channels*

Received for publication, March 22, 2011, and in revised form, September 7, 2011 Published, JBC Papers in Press, September 7, 2011, DOI 10.1074/jbc.M111.237792

Ya-Chin Yang[‡], Shin Lin[§], Po-Chun Chang[§], Hsiao-Chun Lin[§], and Chung-Chin Kuo[§¶1]

From the [‡]Department of Biomedical Sciences and Graduate Institute of Biomedical Sciences, Chang-Gung University, Tao-Yuan 333, the [§]Department of Physiology, National Taiwan University College of Medicine, Taipei 100, and the [¶]Department of Neurology, National Taiwan University Hospital, Taipei 100, Taiwan

Background: The S4 voltage sensor in voltage-gated channels comprises triads of amino acids.
Results: The microenvironment of the S3–4 linker is also arranged in similar triads.
Conclusion: S4 initially moves in a canal following the S3–4 linker but may subsequently take a more liberal move like a paddle.
Significance: This provides a novel synthesis reconciling the currently controversial models of S4 movement.

The highly conserved fourth transmembrane segment (S4) is the primary voltage sensor of the voltage-dependent channel and would move outward upon membrane depolarization. S4 comprises repetitive amino acid triads, each containing one basic (presumably charged and voltage-sensing) followed by two hydrophobic residues. We showed that the triad organization is functionally extended into the S3–4 linker right external to S4 in Shaker K^+ channels. The arginine (and lysine) substitutes for the third and the sixth residues (Ala-359 and Met-356, respectively) external to the outmost basic residue (Arg-362) in S4 dramatically and additively stabilize S4 in the resting conformation. Also, Leu-361 and Leu-358 play a very similar role in stabilization of S4 in the resting position, presumably by their hydrophobic side chains. Moreover, the double mutation A359R/E283A leads to a partially extruded position of S4 and consequently prominent closed-state inactivation, suggesting that Glu-283 in S2 may coordinate with the arginines in the extruded S4 upon depolarization. We conclude that the triad organization extends into the S3–4 linker for about six amino acids in terms of their microenvironment. These approximately six residues should retain the same helical structure as S4, and their microenvironment serves as part of the "gating canal" accommodating the extruding S4. Upon depolarization, S4 most likely moves initially as a sliding helix and follows the path that is set by the approximately six residues in the S3–4 linker in the resting state, whereas further S4 translocation could be more like, for example, a paddle, without orderly coordination from the contiguous surroundings.

Voltage-gated ion channels constitute the molecular basis underlying electrical signaling in excitable tissues. The fourth transmembrane helix or segment (S4)[2] in each subunit or domain is a conserved voltage-sensing structure among these tetrameric proteins. S4 is comprised of a repetitive triad of one basic (and presumably voltage-sensing) residue followed by two hydrophobic ones. Membrane depolarization (and hyperpolarization) would move S4 and transfer maximally three to four triads (*i.e.* a three to four elementary charge) for an S4 across the membrane field (1–4). S4 movement then leads to gating conformational changes that control the passage of selected ions through a voltage-dependent channel.

Several different models of S4 motion were forwarded based on experimental results and simulation data from structural and functional studies (5). Two major ones are the conventional "helical screw" model and the "paddle" model initiated from crystallographic studies (6–9). The two models predict different moving scales of S4, namely 3–13 Å and 15–20 Å, respectively. Moreover, the screw model stands for sequential interactions of S4 charges with an appropriate microenvironment such as a "gating canal" that accommodates the moving S4, whereas the paddle model suggests a sliding of a helix-turn-helix paddle, which contains parts of S4 and the S3–4 linker as a charged cargo and does not have the foregoing sequential or orderly coordination for the amino acids in S4 (10–13). In other words, the essence of the helical-screw model implies that each of the three residues in a triad may, respectively, move to the corresponding position of its preceding triad like a ratchet, whereas the paddle model implies a large-scale movement of a charged cargo without clearly predefined intermediate steps. Although several modified models have been suggested, a consensus is yet to be reached, and many key questions remain (14–16). Both functional and structural findings agree that two conserved acidic residues (Glu-283 and Glu-293 in Shaker K^+ channels) in S2 may, respectively, act as countercharges of the third and the fourth arginines (Arg-3 and Arg-4) in S4 in the activated state, and the former acidic residue may also interact with the outmost arginine (Arg-1) in S4 in the resting state (11,

* This work was supported by National Science Council, Taiwan, Grants NSC99-2321-B-002-008 (to C.-C. K.) and NSC99-2311-B-182-001-MY3 (to Y.-C. Y.). This work was also supported by National Health Research Institutes, Taiwan, Grant NHRI-EX100-10006NI (to C.-C. K.) and Chang Gung Hospital, Taiwan, Medical Research Project CMRPD170453 (to Y.-C. Y.).
[1] To whom correspondence should be addressed: Dept. of Physiology, National Taiwan University College of Medicine, No. 1, Jen-Ai Rd., 1st Section, Taipei 100, Taiwan. Tel.: 886-2-23123456 (ext. 88236); Fax: 886-2-23964350; E-mail: chungchinkuo@ntu.edu.tw.

[2] The abbreviations used are: S4, the fourth transmembrane segment; IR, fast inactivation-removed; MTSET, methanethiosulfonate ethyltrimethylammonium.

17–22). The existence of these countercharge interactions, however, cannot directly argue for or against either model. For the helical-screw model, it is desirable to have a more systemic perspective on the sequential coordination of the repetitive triads in S4 during channel gating. For the paddle model, a more comprehensive view on the spatial distribution of the negative countercharges, and consequently the pattern of paddle movement, seems mandatory.

Previously, we reported that a hydrophobic residue Leu-361 (which is located just external to the outmost arginine Arg-362 in S4) in the S3–4 linker is important for stabilization of S4 in the resting Shaker K^+ channel (23). Together with a recent report that the gating canal could also be occupied by Ala-359 (24), these findings imply an imperative effect of the external extension of S4 (the S3–4 linker) and/or its microenvironment on the positioning of S4. We therefore did mutational scanning of the S3–4 linker residues in the Shaker K^+ channel. We found that the microenvironment surrounding a short segment (containing approximately six amino acids up to Met-356) external to S4 preserves the "pitch" of repetitive triads, presumably designated to accommodate S4 residues upon channel activation. As a result, the initial outward movement of S4 for roughly two triads may be well confined by a gating canal immediately outside S4. Without such a structuralized microenvironment, the subsequent movement, however, may employ a more "liberal" and probably larger scale path to complete the total transfer of three to four triads (three to four charges) across the membrane field.

EXPERIMENTAL PROCEDURES

Molecular Biology and Expression of Shaker K^+ Channels—The Shaker GH4 K^+ channel cDNA (Shaker H4 channels with the addition of three "silent" restriction enzyme sites and a *Xenopus* α-globin untranslated sequence) was used (23). Point mutations were done with the QuikChange mutagenesis kit (Agilent Technologies) on both the wild-type cDNA and the N terminus (6–46 residues) deleted construct (the fast inactivation-removed or IR channels). Both DNA sequencing and biophysical examination were performed to verify the mutations. The full-length cRNA transcript was then synthesized using the T7 mMESSAGE mMACHINE transcription kit (Applied Biosystems). To isolate oocytes, mature female *Xenopus laevis* frogs were anesthetized by cold water and 1.7 gl^{-1} of tricaine (ethyl 3-aminobenzoate methanesulfonic acid, Sigma) and allowed to recover immediately after the surgery. All animal procedures were under the supervision of Institutional Animal Care and Use Committee in National Taiwan University College of Medicine and College of Public Health and that in Chang Gung University. Defolliculated *Xenopus* oocytes (stage V–VI) were injected with the cRNA transcript and then maintained at 18 °C for 1–5 days before electrophysiological recordings.

Electrophysiological Recordings and Data Analysis—When recording, the oocyte was continuously perfused by ND-96 solution (96 mM NaCl, 4 mM KCl, 1 mM $MgCl_2$, 0.3 mM $CaCl_2$, 5 mM HEPES, pH 7.6). Voltage-sensing and current-passing electrodes were filled with 3 M KCl (serial resistance, 0.1–0.4 megohms). Methanethiosulfonate ethyltrimethylammonium (MTSET, Toronto Research Chemicals) was stocked at −70 °C and was freshly prepared before use. Data were acquired with a two-electrode voltage clamp amplifier (model OC-725C, Warner Instruments) at room temperature (~25 °C) and pCLAMP software and digitized at a 20–100-μs interval using a Digidata 1200 analog/digital interface (MDS Analytical Technologies). The WT data were performed in parallel with the mutant data from time to time, and we found little change of results among batches of oocytes. All averaged data are given as mean ± S.E. To plot the inactivation curves, the oocyte was held at −120 mV and stepped every 3 s to the inactivating pulse for 100 ms and then to a test pulse of 0 mV (or +70 mV for Figs. 4 and 5, where the activation curves may be dramatically positively shifted by mutation) to elicit currents. The peak current after each inactivating pulse is normalized to the maximal peak current and plotted against the voltage (V) of the inactivating pulse. The plot is fitted with a Boltzmann function: $1/(1 + \exp((V - V_{½})/k))$, where $V_{½}$ is the half-inactivating potential, and k is the slope factor. To plot the normalized conductance-voltage curves (activation curves), the oocyte expressing the fast IR variant of the wild-type or mutant Shaker K^+ channel was subjected to a series of test pulses increased by a 10-mV step to elicit K^+ currents. The holding potential was −120 mV. The normalized conductance is obtained from the normalized current increase (to the maximal increase) in each 10-mV step and is plotted against the test-pulse voltage where each 10-mV step begins. The plot is fitted with a Boltzmann function $1/(1 + \exp((V_{½} - V)/k))$. The rising phase of the macroscopic currents of the IR channel and the decay phase of the macroscopic currents of the fast inactivation-intact channel are fitted with monoexponential functions to obtain the activation and inactivation time constants (τ), respectively. For the double-mutant cycle analysis (25) based on the shift of the activation curves in the double mutant and either component single mutant channels, the free energy change ($\Delta\Delta G$) for each mutant is derived from the product of $V_{½}$ and the equivalent gating charges (derived from RT/Fk) in the mutant channel minus that in the wild-type channel (R, T, and F have their usual biophysical meanings). The interaction energy $\Delta\Delta G_{inter}$ is equal to the difference between the $\Delta\Delta G$ of the double mutant channel and the sum of $\Delta\Delta G$ in each of component single mutant channels.

RESULTS

Shaker K^+ Channel with Either Arginine or Lysine Substitution for Leu-358 Is Activated and Inactivated at Much More Hyperpolarized Membrane Potentials—We have previously found that the hydrophobicity of Leu-361, an S3–4 linker residue next to the outmost Arg-362 in S4, is important for stabilization of S4 in the resting Shaker K^+ channel (23). Here, we show that Leu-358, the third residue external to Leu-361, plays a very similar functional role to Leu-361. Exactly analogous to the cases with L361R or L361K mutation, the L358R or L358K mutant channel is activated and inactivated at much more hyperpolarized membrane potentials with apparently less voltage dependence when compared with the WT channel (Fig. 1, *A–C*). The changes are not significantly different between arginine and lysine substitutions, and the shifts of the activation and the inactivation curves are quantitatively similar (Fig. 1, *B* and *C*, see also Fig. 2*E*). The latter finding is consistent with a shifted equilibrium between resting and activated states of the

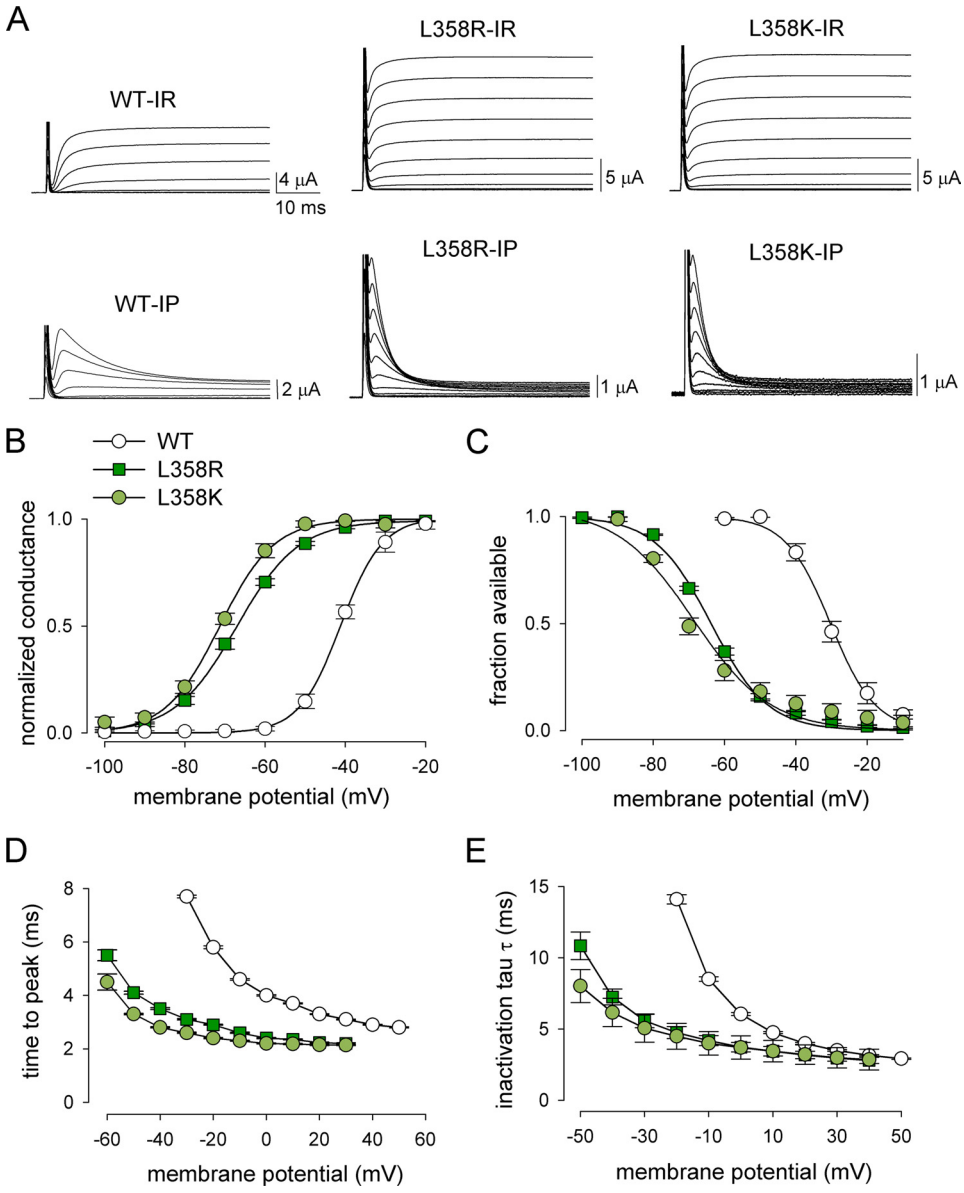

FIGURE 1. **Steady-state curves and kinetics of activation and inactivation in the L358R and L358K mutant channels.** *A*, representative currents through both the fast inactivation-removed (*IR*, *upper row*) and the fast inactivation-preserved (*IP*, *lower row*) variants of the WT and different mutant channels elicited by the same voltage protocol (a series of consecutive depolarization increased by 10 mV from a holding potential of −120 mV). Only raw sweeps that are elicited by test pulses from −100 to 0 mV (increased by 10 mV) are shown here to facilitate comparison. The time scale shown in the *top left panel* applies to all currents in this figure. *B* and *C*, the averaged activation (*B*) and inactivation (*C*) curves of the WT ($n = 14–18$) and the L358R and L358K mutant channels ($n = 6–8$). The curves are the fits with the Boltzmann function (see "Experimental Procedures"). *D* and *E*, macroscopic activation and inactivation kinetics of the WT ($n = 14–18$) and the L358R and L358K mutant channels ($n = 6–8$) at different voltages. The experiments are performed in the inactivation-preserved channels. The oocytes are stepped to the indicated test-pulse voltages from a holding potential of −120 mV to elicit K^+ currents. Because the activation kinetics in the mutant channels are so fast that a reliable exponential fit of the activation phase is difficult, we measured the time to the macroscopic current peak (the time from the beginning of the depolarization step to the current peak) as an indicator of macroscopic activation kinetics (*D*). The monoexponential time constant (τ) of macroscopic current decay is measured to represent the macroscopic inactivation kinetics (*E*). The *lines* connecting the data points are drawn by hand to show the trend of the voltage-dependent change.

mutant channel, based on a simplistic gating model that fast inactivation happens downstream of activation in Shaker K^+ channels. In addition, compared with the WT channel, the macroscopic kinetics of activation and inactivation in both L358R and L358K mutant channels are much faster at relatively negative test voltages but would seem to reach similar saturating rates at more positive pulses (Fig. 1, *D* and *E*). Taken together, these findings suggest a destabilized S4 in the resting L358R and L358K mutant channels, exactly the same as what was proposed for the Leu-361 mutation (23). If the aligned arginine residues in S4 helix are designated as the "R" line, we may have two lines of hydrophobic residues designated as "R−1" and "R+1" lines, respectively. In this regard, both Leu-361 and Leu-358 belong to the R−1 line (see schematic illustration in Fig. 8). The similar findings of Leu-361 and Leu-358 mutations therefore strongly suggest a functional extension of the repetitive triads (and thus the R−1 line) from S4 into the adjacent S3–4 linker. Moreover, the hydrophobic residues in the R−1 line of the S3–4 linker immediately adjacent to S4 may play a critical role in the positioning of S4 in the resting channels.

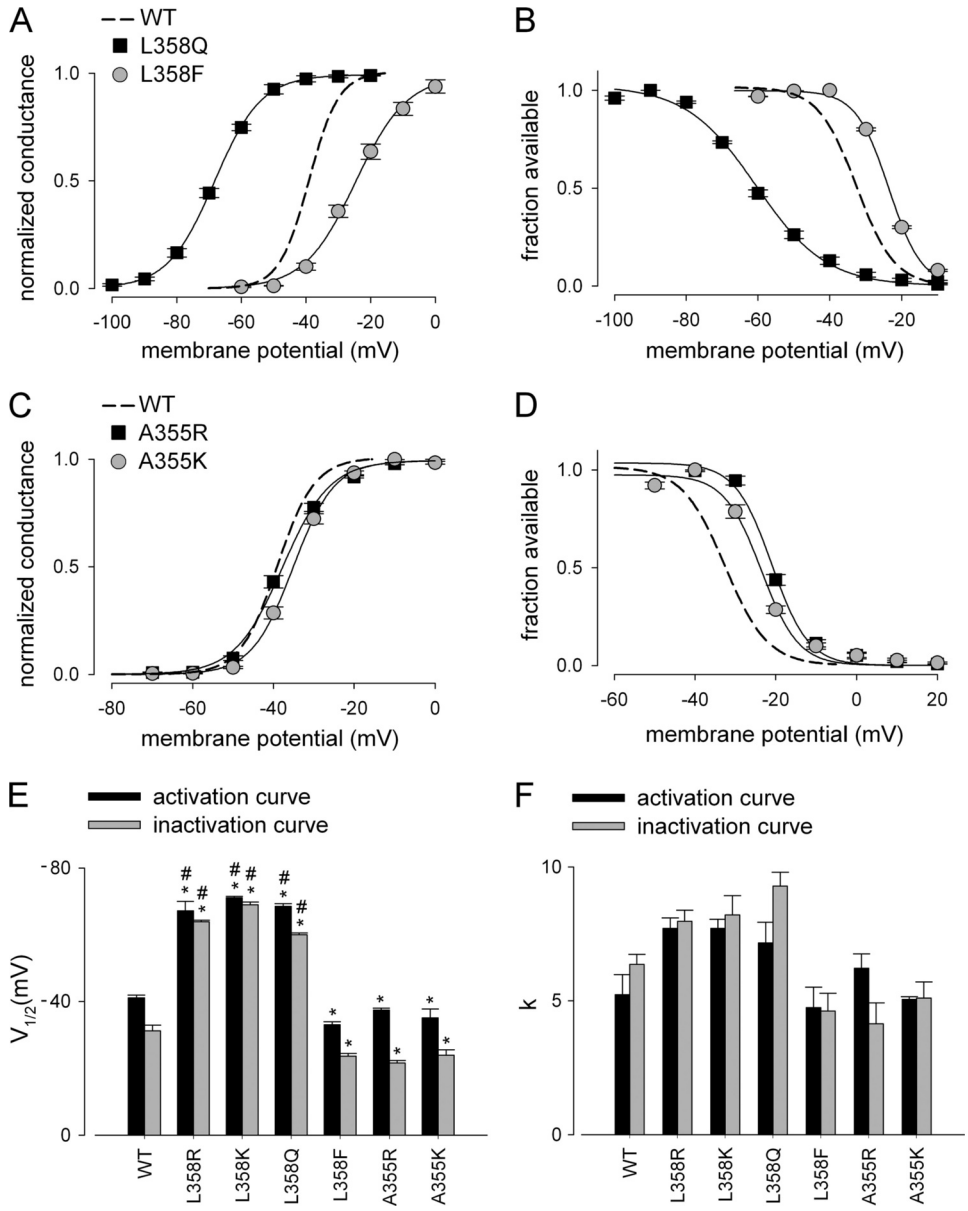

FIGURE 2. **The activation and inactivation curves of the L358Q, L358F, A355R, and A355K mutant channels ($n = 5–6$).** The WT curves are from Fig. 1. *A* and *C*, the averaged activation curves (normalized conductance-voltage curves). The lines are fits of the data with the Boltzmann function. *B* and *D*, the averaged inactivation curves. The *lines* are fits of the data with the Boltzmann function. *E* and *F*, a summary of the averaged $V_{1/2}$ (*E*) and *k* (slope factor, *F*) values of Boltzmann curves among WT and different mutant channels in Figs. 1 and 2. *, $p < 0.01$ compared with the WT data using one-way analysis of variance followed by the Bonferroni's multiple comparison test. #, the averaged shift between the WT and mutant curves is larger than 10 mV. Because the *k* value is only a rough estimate of the gating changes from the fitting curve and is in general varied within a reasonable small range of 5–8, the values are reported without further statistical analysis.

Activation and Inactivation Curves Are Similarly Altered by L358Q but Not by L358F, A355R, or A355K Mutations—We further documented possible changes in the activation and inactivation curves by other substitutions for Leu-358. Again, similar to the cases of Leu-361 (23), neutral hydrophilic glutamine substitution for Leu-358 causes shallower and leftward-shifted activation and inactivation curves. The quantity of shift (~30 mV) is almost the same as that by L358K or L358R (Fig. 2, *A*, *B*, and *E*). On the other hand, neutral hydrophobic substitution such as L358F only slightly shifts the activation and inactivation curves rightward. These findings support a similar contribution of R−1 line residues, Leu-358 and Leu-361, to channel gating, possibly via hydrophobic interaction between leucine and the microenvironment. It seems that the explicit triad organization of amino acid residues in S4 implicitly extends into the S3–4 linker in terms of the organization of the "S4 canal," presumably serving to accommodate an extruded S4 upon depolarization. In this regard, there is only minor or negligible change (shifts smaller than 10 mV considered as energetically negligible change) in the activation and inactivation curves with either A355K or A355R mutations (Fig. 2, *C–E*), suggesting that the "implicit triads" in the S4 canal do not reach the level of Ala-355.

A359R and M356R Mutant Channels Are Activated and Inactivated at Evidently More Depolarized Potentials—In light of the findings of functional extension of the R−1 line into the

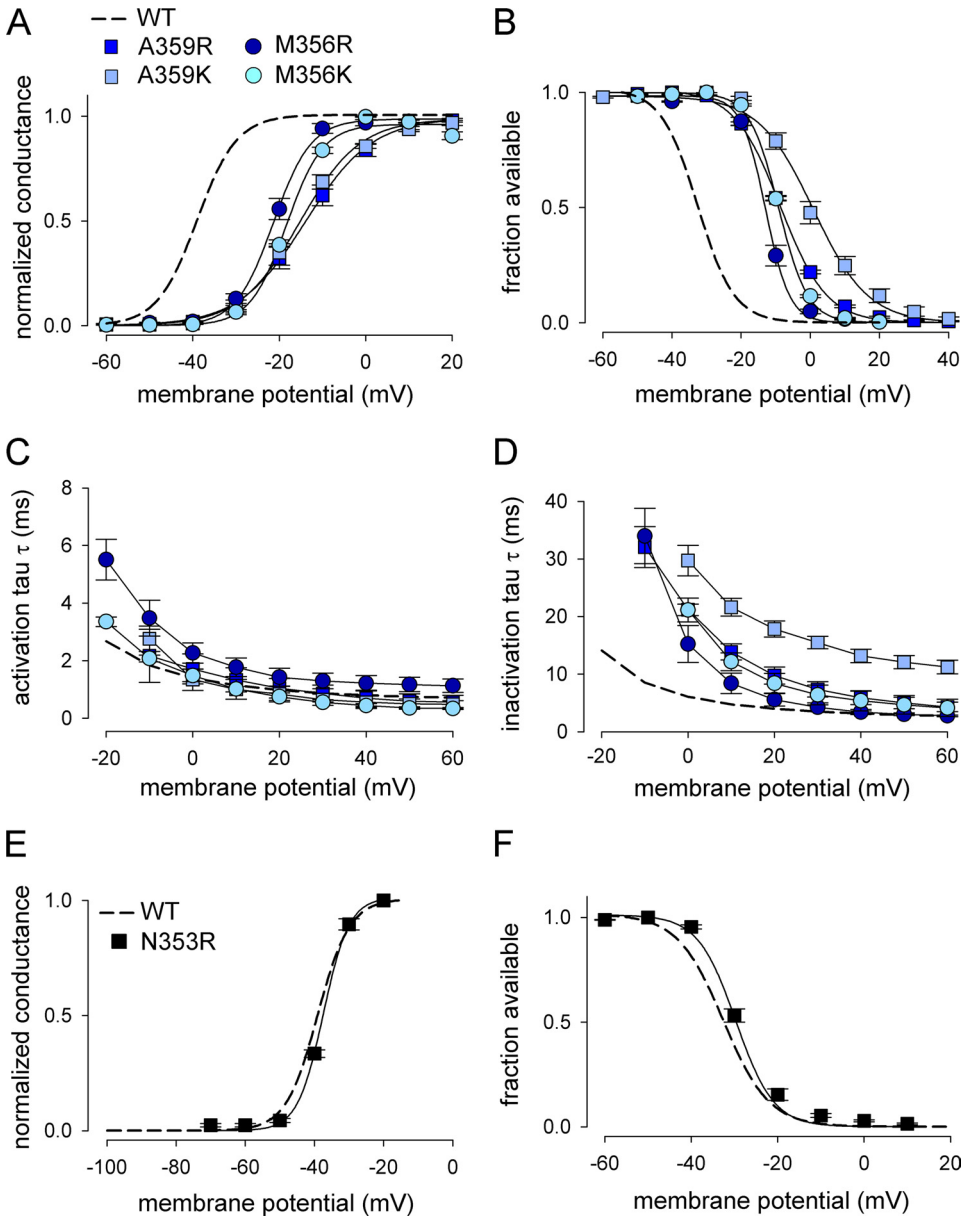

FIGURE 3. **The steady-state gating curves and kinetics in the A359R, A359K, A356R, A356K, and N353R mutant channels ($n = 4–8$).** The WT curves are from Fig. 1. *A* and *B*, the activation and inactivation curves. The *lines* are fits of the data with the Boltzmann function. *C* and *D*, macroscopic activation and inactivation kinetics at different voltages. The gating kinetics are evidently slower in A359R, A359K, A356R, and A356K mutant channels compared with the WT channel (see *A* for the meanings of symbols). *E* and *F*, the activation and inactivation curves of the N353R mutant channel ($n = 5–8$). The *lines* are fits of the data with the Boltzmann function.

S3–4 linker, we then examined whether this extension is also the case for the R line, presumably the main voltage-sensing part in S4. We made arginine and lysine substitutions for Ala-359 and Met-356, the third and the sixth residues external to Arg-362 (the outmost arginine in S4), respectively. In contrast to the prominent leftward shift of the gating curves with arginine or lysine in the extended R−1 line, arginine or lysine substitution for either Met-356 or Ala-359 shifts both the activation and inactivation curves rightward by ~20 mV in the voltage axis (Fig. 3, *A* and *B*, see also Fig. 4*F*). Moreover, both macroscopic activation and inactivation rates are slowed rather than accelerated over a wide range of test voltages (Fig. 3, *C* and *D*). These data are consistent with the idea that the addition of a positive charge in the immediate external extension of the R line would help stabilize the S4 voltage sensor in the resting state (presumably a retracted position of S4). Thus, the repeating triplet organization of the S4 canal once more seems to extend beyond S4 and into the adjacent S3–4 linker. Because arginine substitution for Asn-353 has little effect on the activation and inactivation curves (Fig. 3, *E* and *F*), the R line extension probably ends at Met-356. This would indicate a functional extension of the triplet organization beyond S4 for two more repeats, consistent with the finding for the R−1 line (Fig. 2).

Gating Alterations by A359R and M356R Mutations Are Additive—Positive charge substitutions for Met-356 and those for Ala-359 show quantitatively very similar effects (Fig. 3). To answer the question whether their effects are ascribed to the same (overlapping) or different (separate) molecular interac-

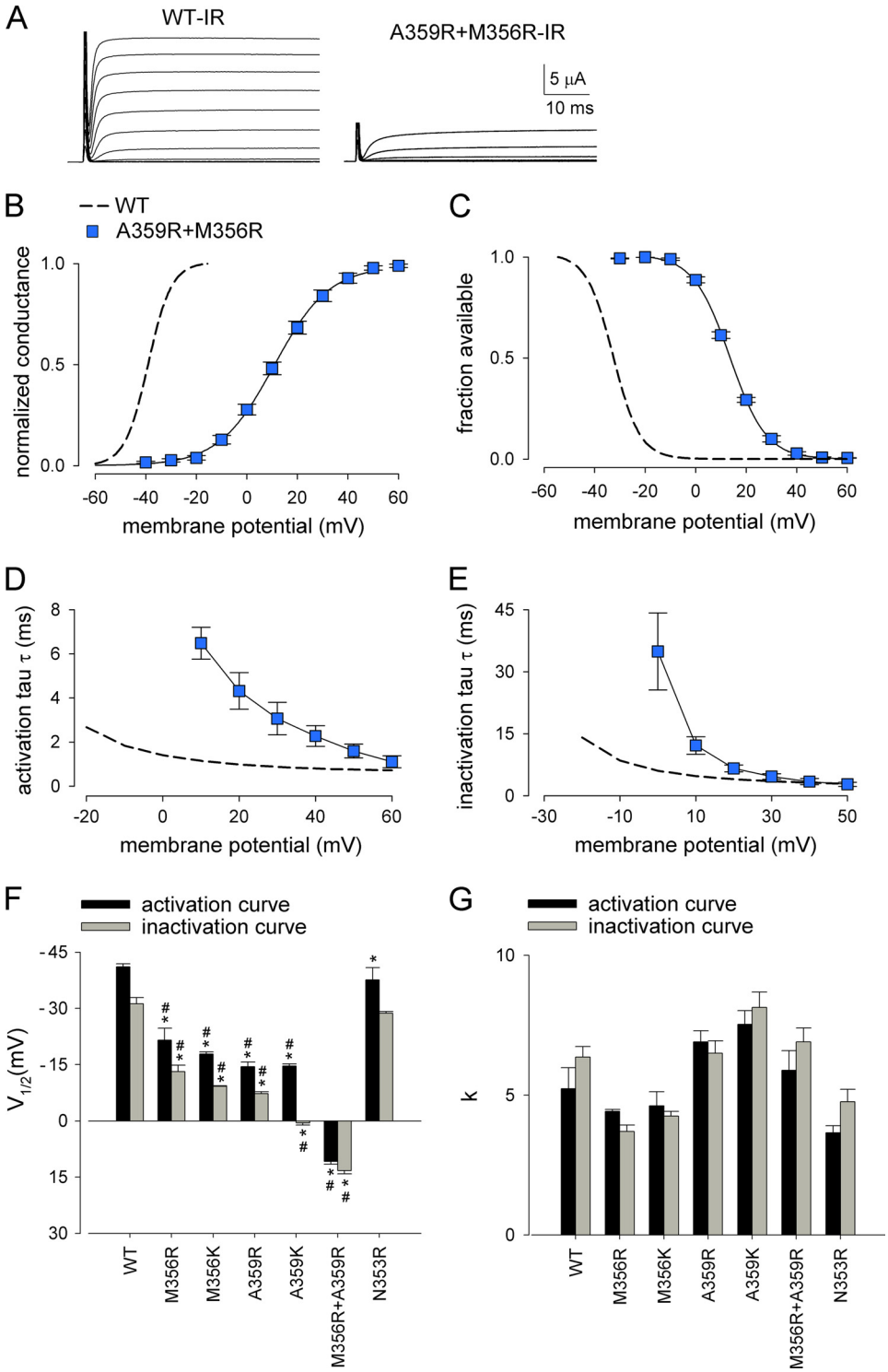

FIGURE 4. **The steady-state gating curves and kinetics in the M356R/A359R double mutant channels (n = 5–7).** The WT curves are from Fig. 1. *A*, representative currents of the fast inactivation-removed (*IR*) WT and M356R/A359R double mutant channels elicited by the same voltage protocol (a series of consecutive depolarization increased by 10 mV from a holding potential of −120 mV). Only raw sweeps that are elicited by test pulses from −100 to +30 mV (increased by 10 mV) are shown here to facilitate comparison. *B* and *C*, the activation and inactivation curves. The *lines* are fits of the data with the Boltzmann function. *D* and *E*, macroscopic activation and inactivation kinetics at different voltages. The gating kinetics of the double mutant channels are much slower than those in the WT channels. *F* and *G*, comparison of the averaged $V_{1/2}$ (*E*) and *k* (*F*) values of Boltzmann curves among WT and different mutant channels in Figs. 3 and 4. *, $p < 0.01$ compared with the WT data using one-way analysis of variance followed by the Bonferroni's multiple comparison test. #, the averaged shift between the WT and mutant curves is larger than 10 mV. Because the *k* value is only a rough estimate of the gating changes from the fitting curve and is in general varied within a reasonable small range of 4–7, the values are reported without further statistical analysis.

tions, we made a double mutation containing both A359R and M356R. In the A359R/M356R double mutant channels, the activation and inactivation curves are shifted by approximately the sum of the shift by either single mutation (A359R or M356R, Fig. 4, *A–C* and *F*). The additive effect indicates separate or independent interactions of A359 and M356 with their

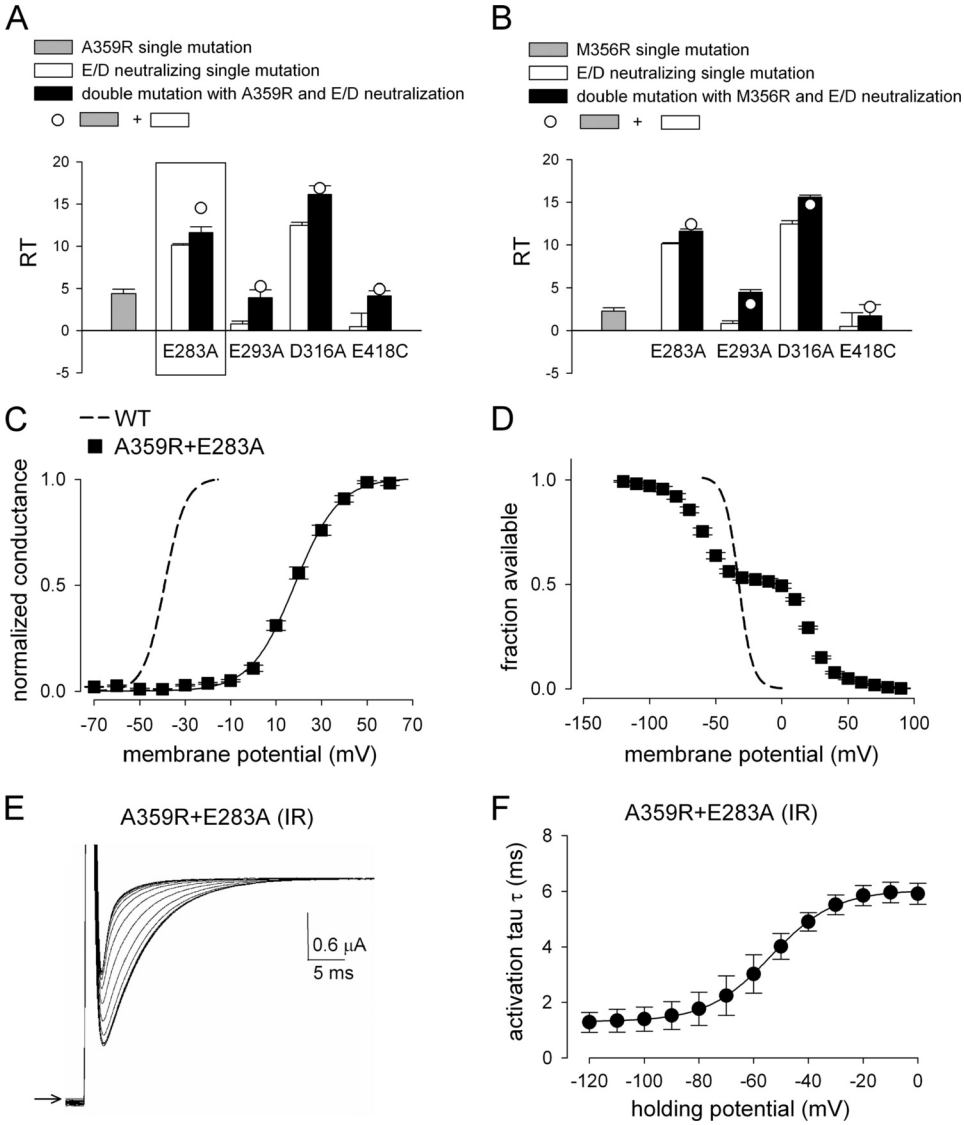

FIGURE 5. **The effect of E283A mutation on the A359R mutant channel.** *A* and *B*, the averaged free energy changes in the double mutant channels involving either A359R (*A*) or M356R (*B*) and in related component single mutant channels are compared in terms of the shift of the activation curve. (For details, see text and "Experimental Procedures;" $n = 5$ for each mutant.) The *open circle* indicates the sum of free energy changes in component single mutant channels. The *rectangle* highlights the largest interaction energy between E283A and A359R. *C* and *D*, the inactivation curve (*D*) but not the activation curve (*C*) is split into two components in the E283A/A359R double mutant channel. The WT curves are from Fig. 1. *E*, the activation rates are paradoxically slowed by more depolarized holding potentials in the IR A359R/E283A channel. The representative currents are elicited by a step depolarization to +70 mV from a series of 300-ms prepulse potentials (−120 mV to 0 mV). Note that the rising phase of the macroscopic currents differs with different prepulse potentials, and the macroscopic activation rate is saturating when the prepulse voltage approaches either −120 mV or 0 mV. The *arrow* indicates zero current level. *F*, the averaged macroscopic activation time constant (τ, measured by an exponential fit of the rising phase of macroscopic currents in *E*) is plotted against the prepulse voltage ($n = 8$). The *line* is the best fit to the data with the Boltzmann function, with a $V_{1/2}$ value of −53.6 mV and a *k* value of 11.6.

respective corresponding environments for stabilization or positioning of S4. Consistently, the kinetics of macroscopic activation and inactivation are much more slowed by the double mutation than the single mutations (Fig. 4, *D* and *E*, compared with Fig. 3, *C* and *D*).

E283A/A359R Double Mutant Channel Shows Biphasic Inactivation Curve and Slowed Activation Kinetics—In search of the corresponding microenvironment that interacts with A359R or M356R (and thus the presumable coordinating ligands for the R line residues during S4 movement), we scanned four acidic residues, Glu-283, Glu-293, Asp-316, and Glu-418, that are previously reported as possible countercharges for the S4 arginines. We neutralized each of the acidic residues, made paired mutations with either A359R or M356R, and then documented the gating changes in the single and double mutant channels. Among the mutations examined, the result of double mutant cycle analysis (see "Experimental Procedures") shows that the largest interaction energy is between E283A and A359R (approximately ~3 RT, consistent with the expected value for a salt bridge between arginine and glutamate side chains, Fig. 5, *A* and *B*). Moreover, only in the E283A/A359R double mutant channel, the inactivation curve is intriguingly split into two parts. This is as if a closed-state inactivation is made manifest (Fig. 5*D*). On the other hand, the activation curve is shifted toward the right but well described by one Boltzmann function with a shallower slope rather than split into two parts (Fig. 5*C*).

These findings can be explained if Glu-283 contributes to the coordination and stabilization of A359R (and S4) in the resting position, presumably via a salt bridge. With neutralization of Glu-283, A359R (and thus S4) probably would tend to move to another energetically favorable substituting microenvironment (*e.g.* another countercharge, see schematic model in Fig. 8). This new, double mutation-caused position of S4 probably stabilizes a closed-state inactivation. In other words, this mutant channel tends to be partially inactivated without significant activation at relatively more hyperpolarized membrane potentials (*e.g.* −60 mV, Fig. 5, *C* and *D*). Further movement of S4 is still required for channel activation and complete inactivation (as inferred by the matched range of membrane potential between the activation curve and the second part of the inactivation curve, Fig. 5, *C* and *D*). This model is consistent with the proposal from previous studies that S4 movement drives a number of closed states before channel opening, although these closed states may not be stable enough to be significantly populated at equilibrium in the wild-type channel (26–30). In this regard, it is interesting that a similar split of the inactivation curve has also been found in Na^+ channels with arginine (and lysine) substitution for Phe-1625, a residue just external to the outmost arginine in S4 of domain 4 (31). In addition, the E283A/A359R double mutant channel shows intriguing prepulse-dependent activation kinetics, supporting the existence of a relatively stabilized intermediate S4 position (and thus a corresponding gating state from which the channel would activate with a slower rate, Fig. 5, *E* and *F*). The macroscopic activation rate paradoxically gets slower with more positive holding potentials between −120 and 0 mV. This change of the activation rate by prepulse potential is saturating at the two ends of the potential range and is well described by a two-state Boltzmann distribution (Fig. 5*F*), which falls well within the voltage range of the first one (the more negative one) of the two Boltzmann distributions of the inactivation curve (Fig. 5*D*). These kinetic and steady-state features altogether are consistent with the proposal that, in addition to an "early" closed state, there is also a "late" closed state stabilized by the E283A/A359R double mutation. This late closed state is associated with partial inactivation (unavailability) of the channel. Moreover, channel activation from this state is paradoxically slower than that from the early closed state (*i.e.* completely deactivated state with fully retracted S4, see below).

Late Closed State Made Manifest by Double Mutation E283A/A359R Is Probably Embodied by Partial Extrusion of S4—To provide a physical picture of S4 in the late closed state made manifest by double mutation E283A/A359R, we added the I364C mutation to the wild-type, E283A single mutant, A359R single mutant, and E283A/A359R double mutant channels. Extracellular methanethiosulfonate (MTSET) reagent readily modifies the I364C/A359R/E283A triple mutant channel at −90 mV in a time-dependent manner (Fig. 6, *A* and *B*). The effect is not large but definite. In contrast, external MTSET has only negligible effect on either the I364C single mutant or the I364C/A359R double mutant channel. I364C/E283A double mutant channels could not produce currents with our expression system. Because external MTSET would modify the sulfhydryl group only if the group was exposed to the extracellular solution, these findings suggest a partial extrusion and/or a change in the secondary structure of S4 in the I364C/A359R/E283A triple mutant channel (18, 32). I364C in the E283A/A359R mutant channel thus is likely exposed to the extracellular milieu at a relatively hyperpolarized membrane potential that would retract S4 and make I364C inaccessible in the wild-type channel (see Fig. 8).

S4 Enters Putative Late Closed State in E283A/A359R Double Mutant Channel with Relatively Voltage-independent Speed of $\sim 250\ s^{-1}$—We have noted that the macroscopic activation rate gets slower with more positive holding potentials between −120 and 0 mV in the E283A/A359R mutant channel (Fig. 5*F*). This slowing seems paradoxical, because activation from the late closed state, where S4 is more protruded intuitively should be faster. One plausible explanation is that the partly protruded S4 in the late closed state is so stabilized as to have an even lower free energy than that in the in the early closed state and thus decreases the speed of further movement of S4 and channel activation. If so, then why would such an activation-slowing effect not be manifest when the channel is activated from the early closed state (as the late closed state should also be traversed before channel opening in this case)? Fig. 7 examines the time courses of the development of the stabilization of the late closed state in the E283A/A359R mutant channel. The macroscopic activation rate is exponentially decreased with lengthening of the prepulse at −40 mV (Fig. 7*A*). The time constant of the exponential decrease is ~4 ms with a prepulse potential of −40 mV and is only equivocally altered by different prepulse voltages (between −40 and −80 mV, Fig. 7*B*). This suggests that S4 enters the late closed state with a relatively slow and voltage-independent speed of $\sim 250\ s^{-1}$. In other words, S4 can only be stabilized in the late closed state if it is held there for at least a few milliseconds. Therefore, during a quick activation process driven by positive pulses from a rather negative holding potential such as −120 mV, there would be no significant stay in the late closed state.

DISCUSSION

Triad Format of Microenvironment Coordinating Repetitive Triads in S4 Extends into S3–4 Linker for Two More Cycles—Fig. 8 shows a schematic illustration of the arrangement of the amino acids in an S4 helix related to the findings in this study. The hydrophobic residues (in the R−1 and R+1 lines) flanking the basic residues in S4 have been classified as high and low impact residues and probably lie in the protein-protein and the protein-lipid (or protein-water) interfaces, respectively, to have different impact on channel gating (13, 33). We found that the S3–4 linker residues Leu-361 and Leu-358 located in the extension of the R−1 line are similarly involved in stabilization of S4 in the resting position (Figs. 1 and 2) (23) and are thus likely facing a similar hydrophobic environment. On the other hand, arginine substitution for Ile-360 and that for Ser-357 in the extension of the R+1 line show only mild and inconsistent effects on channel gating (*e.g.* rightward and leftward shift of the activation curve by ~15 mV for the I360R and S357R mutant channels, respectively, data not shown), consistent with lower impact roles. Moreover, Ala-359 or Met-356 in the extension of the R line no longer carries a positive charge to serve as

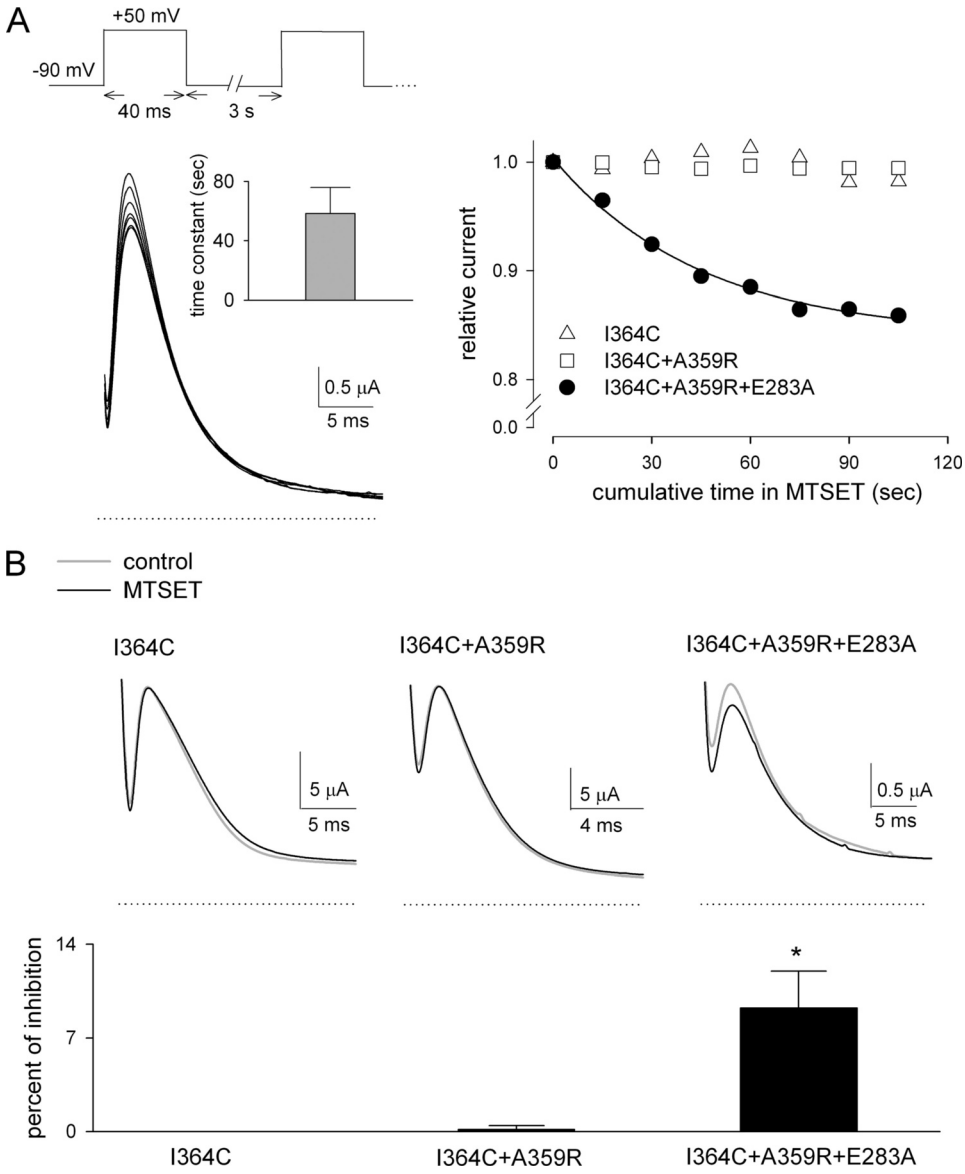

FIGURE 6. **Altered accessibility of I364C to external MTSET in the concomitant existence of A359R/E283A double mutation but not A359R single mutation.** The oocytes expressing the fast inactivation-preserved I364C single mutant, I364C/A359R double mutant, and I364C/A359R/E283A triple mutant channels are held at −90 mV and stepped to +50 mV for 40 ms to elicit current every 3 s. *A*, the representative traces show that the elicited current in the triple mutant channel is decreased with cumulative time in the presence of 1 mM external MTSET. A plot of the sample current amplitude over time relative to that before application of MTSET on the same oocyte is shown in the *right panel*. The decrease of current amplitude with time in the triple mutant channel can be described by a monoexponential function with an average time constant of ~60 s (*inset* of the *left panel*, $n = 4$). In contrast, the I364C single and I364C/A359R double mutant channels do not show any definite responses to MTSET. *B*, the representative raw sweeps (*upper panel*) and the averaged percentage of inhibition (*lower panel*, $n = 3–6$) demonstrate significant decrease in steady-state current amplitude after application of 1 mM external MTSET in the triple but not in the single or the double mutant channels. When the steady-state effect was reached, the oocyte was thoroughly washed with control ND-96 solution. Only the recordings having an irreversible MTSET effect are included. *, $p < 0.01$ for the triple mutant data and $p > 0.5$ for the double mutant data compared with the data of the I364C single mutant channel using one-way analysis of variance followed by the Bonferroni's multiple comparison test. The *dotted line* indicates the zero current level.

a direct voltage sensing element in the wild-type channel. However, they should still face a hydrophilic or even nucleophilic environment as the arginines in S4 do (Figs. 3 and 4) (3, 34, 36, 37). Interestingly, A355R and N353R located in the farther extension of the R−1 and R lines no longer show similar gating effects to those provided by L361R/L358R and by A359R/M356R mutations, respectively (Figs. 2 and 3). The microenvironment designated to accommodate the triad motifs in S4 thus very likely extends into the S3–4 linker for, and only for, another two cycles, and ends right before Ala-355–Asn-353. In other words, the microenvironment that surrounds a short segment of the S3–4 linker immediately external to S4 may serve as part of the S4 canal to coordinate the outwardly moved S4 triads in the activated state. In addition, roughly six residues in the S3–4 linker immediately external to S4 should remain a helical structure. There have been hypotheses that the S4 helix may undergo changes in its secondary structure during movement, such as that part of S4 may adopt 3_{10}-helical structure to provide constraint on S4 residues in the activated position or even it may undergo conversion between 3_{10}-helical and α-helical secondary structure during activation (18, 32). Our findings may further suggest that the C terminus of the S3–4 linker in

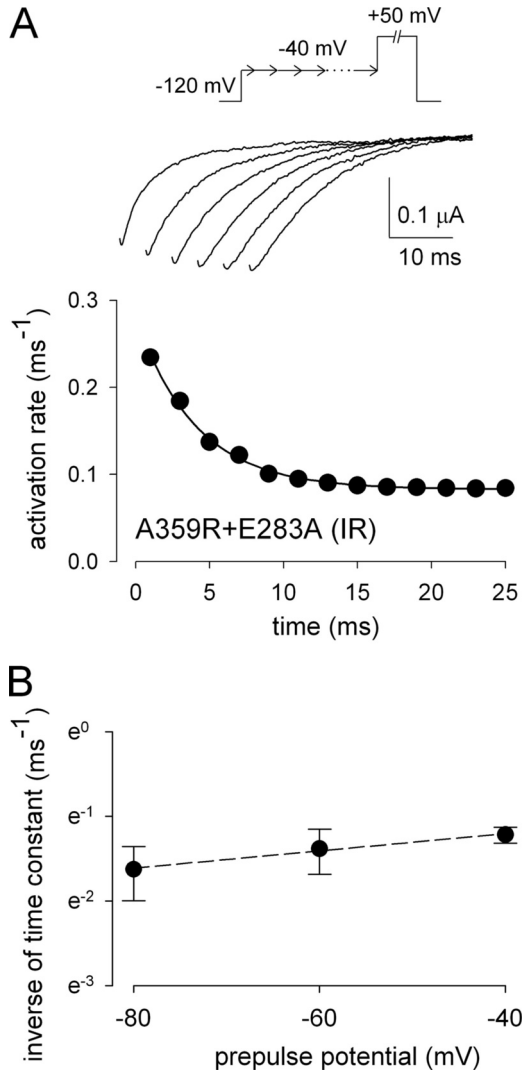

FIGURE 7. **The kinetics of entering the putative late closed state in the A359R/E283A double mutant channel.** *A*, the oocyte expressing the inactivation-removed A359R/E283A double mutant channel is held at −120 mV and stepped to a prepulse at −40 mV for different time intervals ranged from 1 to 25 ms (gradually lengthened by 2 ms) and then stepped to a test pulse of +50 mV to elicit currents. The rising phases of the six elicited macroscopic currents from an oocyte are shown as examples in the *upper panel*. Note the gradual slowing in the macroscopic activation kinetics with lengthening of the prepulse duration. The activation rate (the inverse of the time constant from the best monoexponential fit to the rising phase of current) is plotted against the prepulse duration for this oocyte (the *lower panel*). The line is the best monoexponential fit to the data with a time constant of 4.2 ms. *B*, the same protocol and analysis as that in *A* were repeated with a prepulse voltage of −60 or −80 mV. The kinetics of entering the late closed state (the inverse of time constants in *A*) are not statistically significantly different between prepulses −40, −60, and −80 mV. The *dashed line* defines a very small or even negligible voltage dependence of *e*-fold change per ~100 mV (n = 5–6).

the resting state very likely adopts a similar secondary structure to that of the leading (N-terminal) part of S4 in the activated state; either it is an α or it is a 3_{10}-helical structure.

Leading Part of Fully Protruded S4 May No Longer Stay in Gating Canal of Repetitive Triads—The helical-screw model of S4 movement has two basic features, rotation during activation and relatively stable intermediate states of the voltage sensor (2, 38, 39). The two features may collaborate to make an essential biophysical consequence with the organization of repetitive amino acid triads in S4. With this arrangement, each residue in a triad may move to the corresponding position of the next triad during S4 movement. The disadvantageous free energy gain is then greatly decreased than the case if the basic residues (arginines) would have to traverse the tracks of the flanking hydrophobic residues. In this regard, it is interesting to note the existence of a "S4 gating canal" beside the S3–4 linker contiguous to S4 and also arranged in triad repeats. However, the canal itself does not seem to be long enough to cover the entire movement of S4. In other words, although S4 could move by ~9–12 residues (1–2, 33, 40, 41), the gating canal seems to end at Ala-355–Asn-353. Arg-362 thus needs to move for another 4.5–9 Å (if along the original helical axis) for the fully protruded position of S4. One may surmise that there is still a terminal part of the S4 canal, which would accommodate Arg-362 on the fully protruded S4 but does not accommodate Asn-353 in the resting channel with a fully retracted S4. However, an intriguing possibility would be that, the movement of S4 during activation may be initially a sliding of a less flexible (either α- or 3_{10}-helix) helix, followed by a paddle-like, or other less restricted, movement or even a rearrangement in secondary structure without orderly coordination from its contiguous surroundings. The latter proposal may be further supported by the findings that the leading part of S4 may interact with the pore domain and the S3b segment or even moves close to the peripheral part of the channel protein to interact with the negative charges in the lipid bilayer (9, 42–47).

Glu-283 May Be Responsible for Stabilization of Protruded S4 by Interaction with Basic Residues—It has been suggested that negative charge residues in S2 (Glu-283 and Glu-293), S3 (Asp-316), and S5–S6 pore loop (Glu-418) may be responsible for the stabilization of the outwardly dislocated S4 (11, 17, 48–51). We found that, among the four negative charges, Glu-283 probably plays a role in stabilizing S4 in the resting position at least in the A359R mutant channels. In Fig. 8*C*, we propose a schematic model to explain the possible interactions between the residues in the R line and their microenvironment containing Glu-283. In the S3–4 linker, there are probably countercharges located close to positions Met-356 and Ala-359, respectively, serving to accommodate the arginines in the protruded S4, reminiscent of the fact that S4 prefers a protruded position at 0 mV. In the A359R (or M356R) mutant channel, there is probably one additional charge-charge interaction between A359R and Glu-283 (or between M356R and its counterpart) and thus more stabilization of S4 in the resting (or early closed) state. When Glu-283 is mutated to alanine, this additional stabilization no longer exists. There may be even incompatibility between the arginine (A359R) and alanine (E283A) residues in this local microenvironment. Under such circumstances S4 may have an even stronger tendency to take a partly protruded position (a late closed state) to regain more pairs of interaction (Fig. 8*C*, *middle panel*). On the other hand, the relative tendency to have a more extruded activated position of S4 may be weaker than the case in the wild-type channel (Fig. 8*C*, *right panel*). Because the stabilization of the partly protruded S4 in the E283A/A359R double mutant channel takes milliseconds to develop (Fig. 7), we would propose that the stronger interaction between the arginine at position 359 and its corresponding microenvironment involves significant localizing forces such as hydrogen bonds.

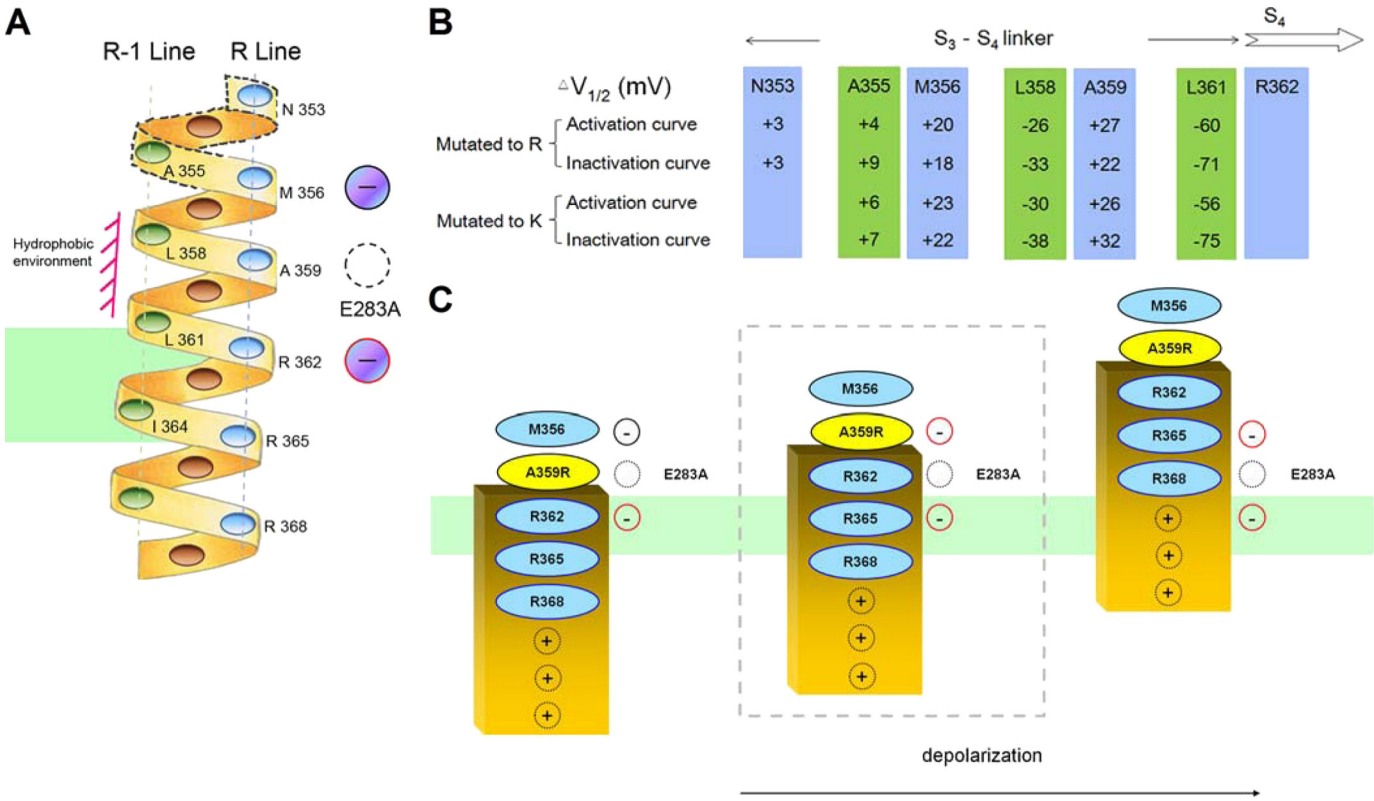

FIGURE 8. *A*, a schematic showing that the amino acids in the S4 helix are arranged in repetitive triads and aligned as R, R−1, and R+1 lines. The helix is drawn with three amino acids per turn for the sake of simplicity in presentation. (There is no intention to designate S4 as a 3_{10}-helical structure, and this figure can be easily redrawn as an α-helix with all of the arguments unchanged.) The relative positions of S4 and presumable countercharges are shown based on a resting channel with fully retracted S4 (see also *C*). The *green bar* denotes the cell membrane. The *filled circles* with *negative signs* and the *dotted circle* (showing the position of E283A) represent the putative microenvironment responsible for coordination of R line residues. *B*, a summary of averaged shifts of gating curves with arginine or lysine substitutions for different S3–4 linker residues. Data are taken from Figs. 2*E* and 4*F* (except that the data for Leu-361 mutations are from Ref. 23). *C*, a schematic model describing the possible interaction of the R line residues with their microenvironment during outward movement of S4. The same rationale may also apply to the microenvironment for the R−1 and R+1 lines (not depicted). S4 is presented as a *gold rectangular bar* with the three outermost arginines (Arg-362, Arg-365, and Arg-368) indicated at its *top*, followed by other R line residues shown as positive signs. The position of S4 residues relative to the cell membrane is consistent with previous findings (4, 35, 55). The other part of the channel that constitutes the S4 gating canal presumably provides negative countercharges or other suitable microenvironment, part of which are shown as negative signs to accommodate the arginines. The *red circles* mark where the interactions with arginines occur. E283A is marked as a *dotted black circle* without a negative sign to designate loss of the countercharge due to mutation. Here, we simplistically illustrate the movement of S4 as translational. Also, in the resting wild-type channel, S4 is depicted to have a pair of charge-charge interaction at its top for simplicity. The argument would remain the same if S4 movement involves rotation and if there are more pairs of interaction. See the text for more details.

This idea provides an explanation for the fact that arginine is much more prevalent than lysine in the voltage sensor S4 and for the dramatic alteration of the activation curve by aspartate substitution for a glutamate residue corresponding to Glu-283 in the Kv7.1 channel (22). If the microenvironment for the triads in S4 does extend into the S3–4 linker for two more cycles, then Glu-283 would likely be located near the external end of the gating canal.

There Is an Intermediate S4 Position Responsible for Partial Inactivation before Channel Opening, Molecular Physiological Implications—We have noted that in the E283A/A359R double mutant channel, the inactivation curve but not the activation curve becomes biphasic (Fig. 5). This finding suggests that a partial outward displaced S4 can cause partial inactivation without opening of the channel. This is consistent with some previously proposed models (26–30, 52). With manipulations of the C-terminal end of the S3–4 linker in domain 4 but not in domains 1–3, we have reported previously profound changes in channel inactivation without any discernible changes in activation in the Na^+ channel and argued that inactivation is delicately and directly controlled by the movement of S4 in domain 4 (31, 53). It is intriguing that partial inactivation may still ensue without channel opening with partly protruded S4 in the Shaker K^+ channel, which has four identical subunits. This finding suggests that the activation-inactivation coupling does not involve the opening of the activation gate itself. Instead, channel inactivation may be even more sensitive to the (early) movement of S4 than activation. In other words, there is very likely a more direct link between S4 and the inactivation gating machinery, at least at relatively hyperpolarized potentials (see review in Ref. 54). The activation-inactivation coupling thus very likely is (at least partly) achieved directly via the S4 movement (53). These principles seem to be well established in Shaker K^+ channels and are mostly preserved in Na^+ channels through the long journey of molecular evolution (except for the specialization of this S4-inactivation gate interaction to S4 in domain 4). Also, if inactivation indeed could proceed before channel opening, and the kinetics of interaction between the R line residues and their countercharges are relatively slow (Fig. 7), then an important functional connotation would be that

slow ramp of increasing depolarization may elicit much less currents through related voltage-dependent channels (such as A-type K^+ channels) than a fast and strong depolarizing pulse. In this regard, it is interesting to imagine that any pharmacological ligands or pathological processes that only mildly alter S4 movement either in speed or in extent may profoundly alter the currents elicited by the same depolarizing pulse, and thus greatly alter the shape of cellular discharges as well as information flow in the neural network.

Acknowledgment—We thank Pei-Yu Chou for help with the artwork in Fig. 8.

REFERENCES

1. Larsson, H. P., Baker, O. S., Dhillon, D. S., and Isacoff, E. Y. (1996) *Neuron* **16,** 387–397
2. Baker, O. S., Larsson, H. P., Mannuzzu, L. M., and Isacoff, E. Y. (1998) *Neuron* **20,** 1283–1294
3. Starace, D. M., and Bezanilla, F. (2001) *J. Gen. Physiol.* **117,** 469–490
4. Yang, N., George, A. L., Jr., and Horn, R. (1996) *Neuron* **16,** 113–122
5. Tombola, F., Pathak, M. M., and Isacoff, E. Y. (2006) *Annu. Rev. Cell Dev. Biol.* **22,** 23–52
6. Catterall, W. A. (1986) *Annu. Rev. Biochem.* **55,** 953–985
7. Catterall, W. A. (1986b) *Trends. Neurosci.* **9,** 7–10
8. Guy, H. R., and Seetharamulu, P. (1986) *Proc. Natl. Acad. Sci. U.S.A.* **83,** 508–512
9. Jiang, Y., Ruta, V., Chen, J., Lee, A., and MacKinnon, R. (2003) *Nature* **423,** 42–48
10. Tiwari-Woodruff, S. K., Schulteis, C. T., Mock, A. F., and Papazian, D. M. (1997) *Biophys. J.* **72,** 1489–1500
11. Tiwari-Woodruff, S. K., Lin, M. A., Schulteis, C. T., and Papazian, D. M. (2000) *J. Gen. Physiol.* **115,** 123–138
12. Durell, S. R., Hao, Y., and Guy, H. R. (1998) *J. Struct. Biol.* **121,** 263–284
13. Li-Smerin, Y., Hackos, D. H., and Swartz, K. J. (2000) *J. Gen. Physiol.* **115,** 33–50
14. Chanda, B., Asamoah, O. K., Blunck, R., Roux, B., and Bezanilla F. (2005) *Nature* **436,** 852–856
15. Pathak, M. M., Yarov-Yarovoy, V., Agarwal, G., Roux, B., Barth, P., Kohout, S., Tombola, F., and Isacoff, E. Y. (2007) *Neuron* **56,** 124–140
16. Tombola, F., Pathak, M. M., Gorostiza, P., and Isacoff, E. Y. (2007) *Nature* **445,** 546–549
17. Papazian, D. M., Shao, X. M., Seoh, S. A., Mock, A. F., Huang, Y., and Wainstock, D. H. (1995) *Neuron* **14,** 1293–1301
18. Long, S. B., Tao, X., Campbell, E. B., and MacKinnon, R. (2007) *Nature* **450,** 376–382
19. Yarov-Yarovoy, V., Baker D., and Catterall, W. A. (2006) *Proc. Natl. Acad. Sci. U.S.A.* **103,** 7292–7297
20. DeCaen, P. G., Yarov-Yarovoy, V., Zhao, Y., Scheuer, T., and Catterall, W. A. (2008) *Proc. Natl. Acad. Sci. U.S.A.* **105,** 15142–15147
21. DeCaen, P. G., Yarov-Yarovoy, V., Sharp, E. M., Scheuer, T., and Catterall, W. A. (2009) *Proc. Natl. Acad. Sci. U.S.A.* **106,** 22498–22503
22. Wu, D., Delaloye, K., Zaydman, M. A., Nekouzadeh, A., Rudy, Y., and Cui, J. (2010) *J. Gen. Physiol.* **135,** 595–606
23. Yang, Y. C., Own, C. J., and Kuo, C. C., (2007) *J. Physiol.* **582,** 1059–1072
24. Gamal El-Din, T. M., Heldstab, H., Lehmann, C., and Greeff, N. G. (2010) *Channels* **4,** 93–100
25. Carter, P. J., Winter, G., Wilkinson, A. J., and Fersht, A. R. (1984) *Cell* **38,** 835–840
26. Schoppa, N. E., and Sigworth, F. J. (1998) *J. Gen. Physiol.* **111,** 271–294
27. Schoppa, N. E., and Sigworth, F. J. (1998) *J. Gen. Physiol.* **111,** 295–311
28. Schoppa, N. E., and Sigworth, F. J. (1998) *J. Gen. Physiol.* **111,** 313–342
29. Ledwell, J. L., and Aldrich, R. W. (1999) *J. Gen. Physiol.* **113,** 389–414
30. Upadhyay, S. K., Nagarajan, P., and Mathew, M. K. (2009) *J. Physiol.* **587,** 3851–3868
31. Yang, Y. C., and Kuo, C. C. (2003) *J. Neurosci.* **23,** 4922–4930
32. Clayton, G. M., Altieri, S., Heginbotham, L., Unger, V. M., and Morais-Cabral, J. H. (2008) *Proc. Natl. Acad. Sci. U.S.A.* **105,** 1511–1515
33. Schönherr, R., Mannuzzu, L. M., Isacoff, E. Y., and Heinemann, S. H. (2002) *Neuron* **35,** 935–949
34. Starace, D. M., Stefani, E., and Bezanilla, F. (1997) Neuron 19, 1319–1327
35. Yang, N., and Horn, R. (1995) *Neuron* **15,** 213–218
36. Tombola, F., Pathak, M. M., and Isacoff, E. Y. (2005) *Neuron* **45,** 379–388
37. Sokolov, S., Scheuer, T., and Catterall, W. A. (2005) *Neuron* **47,** 183–189
38. Cha, A., and Bezanilla, F. (1997) *Neuron* **19,** 1127–1140
39. Glauner, K. S., Mannuzzu, L. M., Gandhi, C. S., and Isacoff, E. Y. (1999) *Nature* **402,** 813–817
40. Mannuzzu, L. M., Moronne, M. M., and Isacoff, E. Y. (1996) *Science* **271,** 213–216
41. Yusaf, S. P., Wray, D., and Sivaprasadarao, A. (1996) *Pflugers Arch.* **433,** 91–97
42. Schmidt, D., Jiang, Q. X., and MacKinnon, R. (2006) *Nature* **444,** 775–779
43. Soler-Llavina, G. J., Chang, T. H., and Swartz, K. J. (2006) *Neuron* **52,** 623–634
44. Jogini, V., and Roux, B. (2007) *Biophys. J.* **93,** 3070–3082
45. Sands, Z. A., and Sansom, M. S. (2007) *Structure* **15,** 235–244
46. Freites, J. A., Tobias, D. J., von Heijne, G., and White, S. H. (2005) *Proc. Natl. Acad. Sci. U.S.A.* **102,** 15059–15064
47. Ramu, Y., Xu, Y., and Lu, Z. (2006) *Nature* **442,** 696–699
48. Planells-Cases, R., Ferrer-Montiel, A.V., Patten, C.D., and Montal, M. (1995) *Proc. Natl. Acad. Sci. U.S.A.* **92,** 9422–9426
49. Seoh, S. A., Sigg, D., Papazian, D. M., and Bezanilla, F. (1996) *Neuron* **16,** 1159–1167
50. Elinder, F., Männikkö, R., and Larsson, H. P. (2001) *J. Gen. Physiol.* **118,** 1–10
51. Zhang, L., Sato, Y., Hessa, T., von Heijne, G., Lee, J. K., Kodama, I., Sakaguchi, M., and Uozumi, N. (2007) *Proc. Natl. Acad. Sci. U.S.A.* **104,** 8263–8268
52. Armstrong, C. M. (2006) *Proc. Natl. Acad. Sci. U.S.A.* **103,** 17991–17996
53. Yang, Y. C., Hsieh, J. Y., and Kuo, C. C. (2009) *J. Gen. Physiol.* **134,** 95–113
54. Bähring, R., and Covarrubias, M. (2011) *J. Physiol.* **589,** 461–479
55. Chahine, M., George, A. L., Jr., Zhou, M., Ji, S., Sun, W., Barchi, R. L., and Horn, R. (1994) *Neuron* **12,** 281–294